Incidence of in situ annealing on the nanoscale topographical/electrical properties of the tunnel barrier in sputtered epitaxial Fe/MgO/Fe multilayers

D J Kim, J Arabski, V da Costa, G Schmerber, M Bowen, S Boukari, E Beaurepaire

Incidence of *in-situ* annealing on the nanoscale topographical/electrical properties of tunnel barrier in sputtered epitaxial Fe/MgO/Fe multilayers

D J Kim, J Arabski, V Da Costa, G Schmerber, M Bowen, S Boukari and E Beaurepaire

IPCMS UMR 7504 CNRS, Université de Strasbourg, 23 Rue du Loess, BP 43, 67034 Strasbourg Cedex 2, France

E-mail: dong-jik.kim@ipcms.u-strasbg.fr (D J Kim) and eric.beaurepaire@ipcms.u-strasbg.fr (E Beaurepaire)

Abstract. Technological improvements in the magnetotranport performance of Fe/MgO/Fe stacks require nanoscale control over the topographical and electrical properties of the ultrathin MgO barrier. We have statistically investigated the incidence of *in-situ* annealing of the lower Fe layer on the nanoscale topographical/electrical properties of Fe/MgO bilayers and the structural and magnetic properties of Fe/MgO/Fe/Co multilayers prepared by sputtering. This annealing step improves the crystal quality of both the lower Fe and upper Fe/Co layers, leading to an enhanced saturated magnetic moment. Finally, this annealing step substantially mitigates the presence of nanohills on the lower Fe layer and improves the uniformity of the height and/or the thickness of MgO tunnel barrier. Our results pave the way for studies of nanoscale transport on micron-sized devices through a better understanding of, and control over, nanoscale hotspots in the tunnel barrier.

PACS numbers: 85.75.Dd, 81.15.-z, 68.55.-a

Submitted to: *J. Phys. D: Appl. Phys.*

1. Introduction

Epitaxial magnetic tunnel junctions (MTJs) that comprise a MgO barrier sandwiched between Fe electrodes have attracted much fundamental and applied interest due to a very high tunneling magnetoresistance (TMR) that reflects the conservation of electron symmetry and spin during the tunneling process [1, 2, 3]. Relative to stacks grown by molecular beam epitaxy, a large TMR at room temperature in sputtered MTJs is a key factor for industrial applications such as high density random access memories or sensitive magnetic sensors. Since the prediction of TMR ratios larger than 1000% in epitaxial Fe/MgO/Fe MTJs [4, 5], there has been much effort to experimentally obtain a high TMR ratio in Fe/MgO/Fe MTJs [6, 8, 7, 9]. However, TMR ratios at room temperature in MgO-based MTJs have reached only 200% with Fe electrodes [9, 10] and 600% with FeCoB alloy electrodes [11].

This discrepancy between the theoretical and experimental TMR ratios is believed to reflect the impact on spin-polarized transport [12] of structural deviations from the ideal multilayer stack, both in the bulk and at the interface. The interface may indeed be fraught with roughness and/or the formation of FeO [13, 14], which are known to degrade the TMR ratio [4]. While the FeCoB/MgO system enjoys strategic standing for technological applications due to the sputtering deposition technique, the choice of substrate (Si) and large TMR values [11], the resulting boron interdiffusion within the MgO barrier [15] impairs a fundamental understanding of the impact of intrinsic MgO defects on the giant TMR effect and its technological implications.

Many reports attest to the importance of high-temperature annealing in promoting the good crystallinity of the Fe/MgO/Fe stack, whether within the bulk of the layers or at the interfaces [16]. This reflects in part the search for a suitable protocol to overcome the 3-dimensional Volmer-Weber growth mode of Fe on MgO due to a large difference in surface energy [17], while limiting any interdiffusion between each layer [18, 19]. We report here on a suitable annealing protocol that yields technologically relevant sputtered Fe/MgO/Fe epitaxial multilayers with improved structural and magnetic properties by annealing *in-situ* the lower Fe layer before the MgO barrier deposition. Our nanoscale statistical analysis of the topography and electrical transport across the ultrathin barrier yields valuable insights into mechanisms on the nanoscale that drive the transport properties of micron-sized devices.

2. Experimental details

We sputtered our Fe/MgO/Fe multilayers on MgO(001) single-crystal substrates in an ultrahigh vacuum (UHV) multichamber system with UHV sample transfer capability. The base pressure was 3.0×10^{-9} mbar. MgO substrates were cleaned with acetone and ethanol, and then inserted into the multichamber system and annealed at 600°C in UHV for 1 hour to clean the surface and remove carbon compounds. We then rf-sputtered a 10-nm thick MgO buffer layer onto the substrate to sequester any carbon from the substrate.

Subsequently, Fe(20 nm, lower)/MgO(2.1 nm)/Fe(10 nm, upper) were deposited at room temperature by dc-, rf-, and dc-magnetron sputtering, respectively. Deposition rates were 1.7 nm/min for Fe and 0.47 nm/min for MgO. The Ar pressure during sputtering was 1.2×10^{-3} mbar. To improve the structural and magnetic properties of the multilayer stack, we annealed some of our samples in UHV at 550°C for 1 hour after the growth of the lower Fe layer and before depositing the MgO barrier. These are hereafter called 'annealed' samples relative to their 'non-annealed' counterparts. Subsequently, we deposited a 25 nm-thick Co layer by UHV thermal evaporation with a effusion cell to magnetically harden the upper Fe layer, and capped all samples with thermally evaporated Au to avoid oxidation.

After all deposition, we performed structural, magnetic and topographical/electrical investigations using a monochromatic x-ray diffractometer (XRD; Siemens D5000), an alternating gradient force magnetometer (AGFM; Princeton Measurements Corporation MicroMag Model 2900), and a conductive-tip atomic force microscope (CT-AFM; Digital Instruments Dimension 3100). Our CT-AFM studies, which were performed using a commercial PtIr-coated cantilever, yield topographical and electrical maps on the nanoscale of the surface that, together, can provide useful information on the structural and electrical quality of a tunnel barrier, such as the presence of nanoscale electrical hotspots [20, 21].

3. Results and discussion

We present $\theta-2\theta$ scans of annealed and non-annealed samples in Fig. 1(a). The Fe(200) and Co(110) peaks indicate that the Fe and Co layers in both samples are well-ordered epitaxially with bcc and hcp structures, respectively [8, 22]. Given the absence of any other peaks in the pattern, we infer that the upper Fe layer is also epitaxial. This in turn implies that, although we cannot distinguish the ultrathin MgO barrier from the substrate signal, the MgO barrier is also epitaxial. Additional phi scans (not shown here) confirm the well-known orientation relation Fe(100)[001]/MgO(100)[110] for our samples. The lattice constant of Fe(200) increased 0.43% and that of Co(110) decreased 0.14% due to annealing, with both tending toward bulk values. These changes in lattice parameters are explained by a thermally-induced relaxation of strain in the Fe layers that impacts the lattice parameter of the Co layer on top. The Fe(200) and Co(110) peaks in $\theta-2\theta$ scans of the annealed sample are more intense with a lower background than those of the non-annealed samples, which reflects an improved crystallinity of the Co and upper/lower Fe layers.

We present in Fig. 1(b) the applied magnetic field (H) dependence of the magnetic moment per unit area (M) for both non-annealed and annealed samples with a 2.1 nm-thick MgO barrier. Both sample types exhibit an abrupt magnetization reversal and a clear magnetic decoupling of the lower and upper magnetic layers, as confirmed by the minor loops presented in the inset. These data show how annealing leads to an increase in M at saturation, which can be interpreted as an improvement in the crystallinity of

the Fe and Co layers, consistently with the aforementioned XRD results.

We present in Fig. 2 the topographical and local current maps obtained on non-annealed samples, revealing the presence of many nanohills on the ultrathin MgO layer. These topographical defects are associated in the local current map with nanoscale hotspots: the current through the nanohills was a few nA or reached the saturation of preamplifier. Because Fe films on MgO surfaces follow a Volmer-Weber growth mode at room temperature due to a big difference in surface energy, one expects the presence of many Fe islands on MgO that grow bigger and coalesce with increasing Fe thickness. We indeed find that samples with a 60 nm-thick lower Fe layer exhibit larger but fewer nanohills than those with a 20 nm-thick lower Fe layer. This means that these nanohills originate from the Fe layer and not the overlying ultrathin MgO layer. We presume that a MTJ stack that integrates a tunnel barrier with such nanohills would lead to a degraded $k_{//}$ conservation of the electron wavefunctions and thus to a significantly reduced TMR [4, 5].

In contrast to the rough topography and associated current hotspots found on the non-annealed samples, the annealed samples obtained by annealing the lower Fe layer prior to the MgO deposition exhibit virtually no nanohills nor current nanoscale hotspots as has been reported on MBE-grown samples [8]. To back this claim, we present in Fig. 3(a) $\sim$ 3(d) topographical/current maps that are representative of the multiple scans performed on different areas of the annealed samples. Furthermore, the rms-roughness found on the MgO/Fe/MgO stack is 0.24 nm, which is nearly the same as that of the substrate. The periodic stripes in Fig. 3(b) reflect background noise of less than 20 pA, implying no detectable tunneling current at 2.5 mV bias. We believe that annealing the entire stack after deposition would not eliminate the rough topography and associated current hotspots to the extent that our annealing procedure on the lower Fe layer does.

To check the electrical quality of the MgO tunnel barrier, we mapped the tunneling current for an annealed sample with a higher bias of 1.0 V as shown in Fig. 3(d), and calculated statistical distributions of local currents from the current image maps of annealed and non-annealed samples [see Fig. 4(a)]. As reported previously [20], the high-bias tunneling current for our annealed samples is inhomogeneous and is not correlated to the topography of Fig. 3(c). This reflects spatial deviations in the effective barrier height and/or barrier thickness. The local current distribution in non-annealed samples exhibits a long tail, which represents the very large current through the barrier and corresponds to the nanoscale hotspots. On the contrary, the local current distribution in annealed samples shows a much narrower and faster-decaying current dependence. This indicates that the MgO tunnel barrier in annealed samples has more uniform height/thickness of MgO tunnel barrier than those in non-annealed samples [20, 21].

The broad distribution of tunneling current originates from small spatial fluctuations of tunnel barrier parameters, such as a barrier height and a barrier thickness [23]. Although we considered only fluctuations of the barrier thickness in the following discussion, which means that the barrier height is assumed to be a constant in the

considered area, our approach can conversely address fluctuations in barrier height due to a constant barrier thickness since both parameters enter exponentially into the expression of the tunneling current. The tunneling current i depends exponentially on the barrier thickness l:

$$i = i_0 e^{-l/\lambda}, \tag{1}$$

where λ is the attenuation length. The expression of λ depends on the value of the voltage V with respect to the barrier height ϕ [24]. In our experiments we applied 1 V to the barrier to get a sizeable current, so that we expect $V > \phi/e$ and

$$\lambda = \frac{0.74\hbar eV}{\sqrt{2m\phi^3}}, \tag{2}$$

where m is the electron mass. In the Gaussian distribution of the barrier thickness l with a mean μ_l and a standard deviation σ_l, this leads to a lognormal distribution $P(i)$ of tunneling current i:

$$P(i) = \frac{1}{i\sqrt{2\pi\sigma^2}} \exp\left(-\frac{(\ln i - \mu)^2}{2\sigma^2}\right), \tag{3}$$

where $\mu = \mu_l/\lambda + \ln i_0$ and $\sigma^2 = (\sigma_l/\lambda)^2$, and $\sigma_l^2 = \sigma_{\mathrm{MgO}}^2 + \sigma_{\mathrm{Fe}}^2$. $\sigma_{\mathrm{MgO(Fe)}}$ is a standard deviation of topographical fluctuation in the MgO(Fe) layer [20, 21]. Using the above formalism, we confirm that the topographical fluctuations of MgO barrier and lower Fe layer follow a Gaussian distribution with $\sigma_{\mathrm{MgO}} = 0.21$ nm [see Fig. 4(b)] and $\sigma_{\mathrm{Fe}} = 0.15$ nm [see Fig. 4(c)].

Referring to Fig. 4(a), line 1 is the best fit of the current distribution in the annealed sample, while lines 2 and 3 simulate the current distribution when fluctuations of MgO barrier thickness are 1.5 times and 3 times larger, respectively, than the annealed sample with the fixed other parameters. Taking into account the measured topographical fluctuations of the MgO barrier in the annealed sample, we obtain an effective barrier height in the annealed sample of 0.78 eV at 1.0 V, which is in line with Bowen *et al* 's result of 0.9 eV [6] and higher than that found by Yuasa *et al* [9]. The presence of metal-induced gap states across the ultrathin layer [25], with a reduced band gap [4] relative to the bulk, may explain why all these reported barrier heights remain much lower than the ideal value of 3.6 eV for bulk MgO. The fact that the estimated barrier height agrees with the above criterion ($V > \phi/e$) validates our analysis.

Relative to the annealed sample, we note how a current distribution fit using fluctuations in the barrier thickness that are 3 times larger can yield a reasonable agreement with the current distribution in the non-annealed sample [see line 3 of Fig. 4(a)]. Since both the MgO barrier thickness and barrier height are fluctuating in the non-annealed sample due to the apparent conductive nanohills in the CT-AFM data, we may conclude that the observed power-law-like behavior of the current distribution results from a very broad distribution of barrier height/thickness [see Fig. 2(f) in Ref. 20].

From the equation of the log-normal distribution, the average current values $<i> = \exp(\mu + \sigma^2/2)$ in the considered area are 29 pA in the annealed sample and

3.6 nA in the non-annealed sample. With these values and tip radius ($\sim$ 25 nm), we obtain resistance $\times$ area (RA) values of $6.8 \times 10^7\ \Omega \cdot \mu\text{m}^2$ in the annealed sample and $5.5 \times 10^5\ \Omega \cdot \mu\text{m}^2$ in the non-annealed sample. The RA value in the annealed sample is much larger than that in the non-annealed sample, which underscores the electrical impact of the nanohills and nanoscale hotspots in the latter case. Both sample types exhibit a RA product that is two orders of magnitude larger than that reported in the literature [9]. Despite RA product differences observed in these two sample types, we observe good magnetic decoupling, which attests to the continuity of the MgO barrier layer.

4. Conclusion

In summary, we have studied the growth, structure, magnetism and interface morphology of epitaxial Fe/MgO/Fe/Co multilayers grown onto MgO(001) substrates. Samples with a lower Fe deposited at room temperature exhibit conductive nanohills through the MgO barrier. On the other hand, vacuum annealing prior to the MgO barrier deposition improves both the crystallinity of the whole stack, the magnetization of the layers, and leads to a MgO barrier surface roughness of 0.24 nm on par with the 0.20 nm rms-roughness found on the underlying MgO substrate. Our annealing protocol can thus help improve the structural quality of sputtered epitaxial Fe/MgO/Fe stacks as well as the uniformity of MgO barrier height/thickness. We expect that this fundamental growth study and statistical analysis in a nanoscale can contribute to bridging the gap between theory and experiment in the Fe/MgO system through improvements in the quality of the epitaxial stack. Considering that the current across micron-sized junctions shall proceed almost entirely through nanoscale hotspots, our work shows how, on a microscopic junction with a surface area of 1 μm^2 that is processed from a suitably grown stack, current will proceed through between 3 and 6 nanoscale hotspots. Our work should help understand transport in micron-sized tunnel junction in terms of tunneling across a number of nanoscale junctions.

Acknowledgments

This research was supported by the EC Sixth Framework Program (Contract No. NMP3-CT-2006-033370) and by the French National Research Agency (Contract No. ANR-06-NANO-033-01).

References

[1] Nagahama T and Moodera J S 2006 *J. Magn.* **11**, 170
[2] Greullet F, Tiusan C, Montaigne F, Hehn M, Halley D, Bengone O, Bowen M and Weber W 2007 *Phys. Rev. Lett.* **99**, 187202
[3] Yuasa S and Djayaprawira D D 2007 *J. Phys. D: Appl. Phys.* **40**, R337
[4] Butler W H, Zhang X-G, Schulthess T C and Maclaren J M 2001 *Phys. Rev. B* **63**, 054416

[5] Mathon J and Umerski A 2001 *Phys. Rev. B* **63**, 220403R
[6] Bowen M, Cros V, Petroff F, Fert A, Martínez Boubeta C, Costa-Krämer J L, Anguita J V, Cebollada A, Briones F, de Teresa J M, Morellón L and Ibarra M R 2001 *Appl. Phys. Lett.* **79**, 1655
[7] Faure-Vincent J, Tiusan C, Jouguelet E, Canet F, Sajieddine M, Bellouard C, Popova E, Hehn M, Montaigne F and Schuhl A 2003 *Appl. Phys. Lett.* **82**, 4507
[8] Popova E, Faure-Vincent J, Tiusan C, Bellouard C, Fischer H, Hehn M, Montaigne F, Alnot M, Andrieu S, Schuhl A, Snoeck E and da Costa A 2002 *Appl. Phys. Lett.* **81**, 1035
[9] Yuasa S, Nagahama T, Fukushima A, Suzuki Y and Ando K 2004 *Nat. Mater.* **3**, 868
[10] Yuasa S 2008 *J. Phys. Soc. Jpn.* **77**, 031001
[11] Ikeda S, Hayakawa J, Ashizawa Y, Lee Y M, Miura K, Hasegawa H, Tsunoda M, Matsukura F and Ohno H 2008 *Appl. Phys. Lett.* **93**, 082508
[12] Halley D, Majjad H, Bowen M, Najjari N, Henry Y, Ulhaq-Bouillet C, Weber W, Bertoni G, Verbeeck J and Van Tendeloo D 2008 *Appl. Phys. Lett.* **92**, 212115
[13] Yu B D and Kim J-S 2006 *Phys. Rev. B* **73**, 125408
[14] Heiliger C, Zahn P, Yu Yavorsky B and Mertig I 2006 *Phys. Rev. B* **72**, 180406
[15] Lu Y, Tran M, Jaffres H, Seneor P, Deranlot C, Petroff F, George J-M, Lepine B, Ababou S and Jezequel G 2009 *Phys. Rev. Lett.* **102**, 176801
[16] Ikeda S, Hayakawa J, Lee Y M, Tanikawa T, Matsukura F and Ohno H *J. Appl. Phys.* **99**, 08A907
[17] Lee J, Dreyer M, Krafft C and Gomez R D 2007 *J. Appl. Phys.* **101**, 09D123
[18] Cardoso S, Freitas P P, de Jesus C, Wei P and Soares J C 2000 *Appl. Phys. Lett.* **76**, 610
[19] Schmalhorst J, Brückl H, Justus M, Thomas A, Reiss G, Vieth M, Gieres G and Wecker J 2001 *J. Appl. Phys.* **89**, 586
[20] Da Costa V, Henry Y, Bardou F, Romeo M and Ounadjela K 2000 *Eur. Phys. J. B* **13**, 297
[21] Da Costa V and Romeo M 2006 *Adv. Sci. Technol.* **52**, 116
[22] Wang S G, Wang C, Kohn A, Lee S, Goff J P, Singh L J, Barber Z H and Ward R C C 2007 *J. Appl. Phys.* **101**, 09D103
[23] Bardou F 1997 *Europhys. Lett.* **39**, 239
[24] Simmons J G 1963 *J. Appl. Phys.* **34**, 1793
[25] Bowen M, Barthélémy A, Bellini V, Bibes M, Seneor P, Jacquet E, Contour J-P and Dederichs P H 2006 *Phys. Rev. B* **73**, 140408(R)

Figure captions

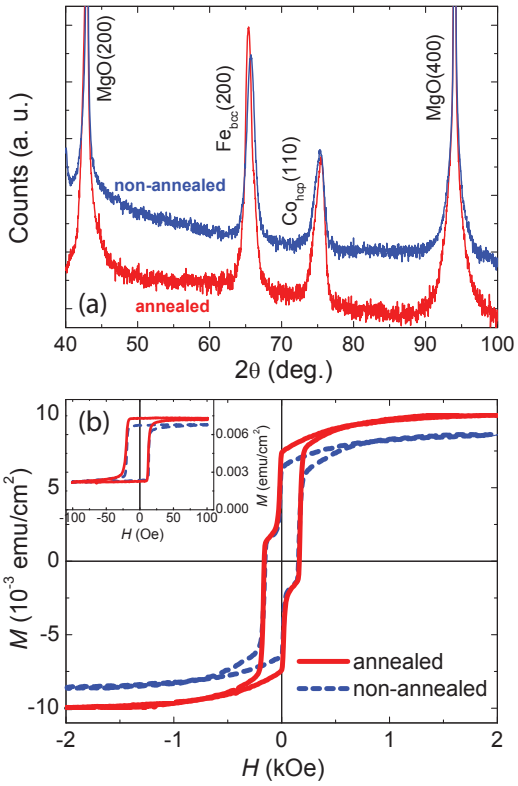

Figure 1. (a) $\theta - 2\theta$ scans for annealed and non-annealed MgO/Fe/MgO/Fe/Co/Au stacks on MgO substrates, using Cu-Kα_1 radiation. (b) Magnetic hysteresis loops measured by AGFM at room temperature. The solid red (dashed blue) line shows magnetization per unit area in annealed (non-annealed) samples. The loops were acquired with an external magnetic field parallel to the Fe(100) easy axis (MgO[110] // Fe[100]). Inset: minor magnetization loops.

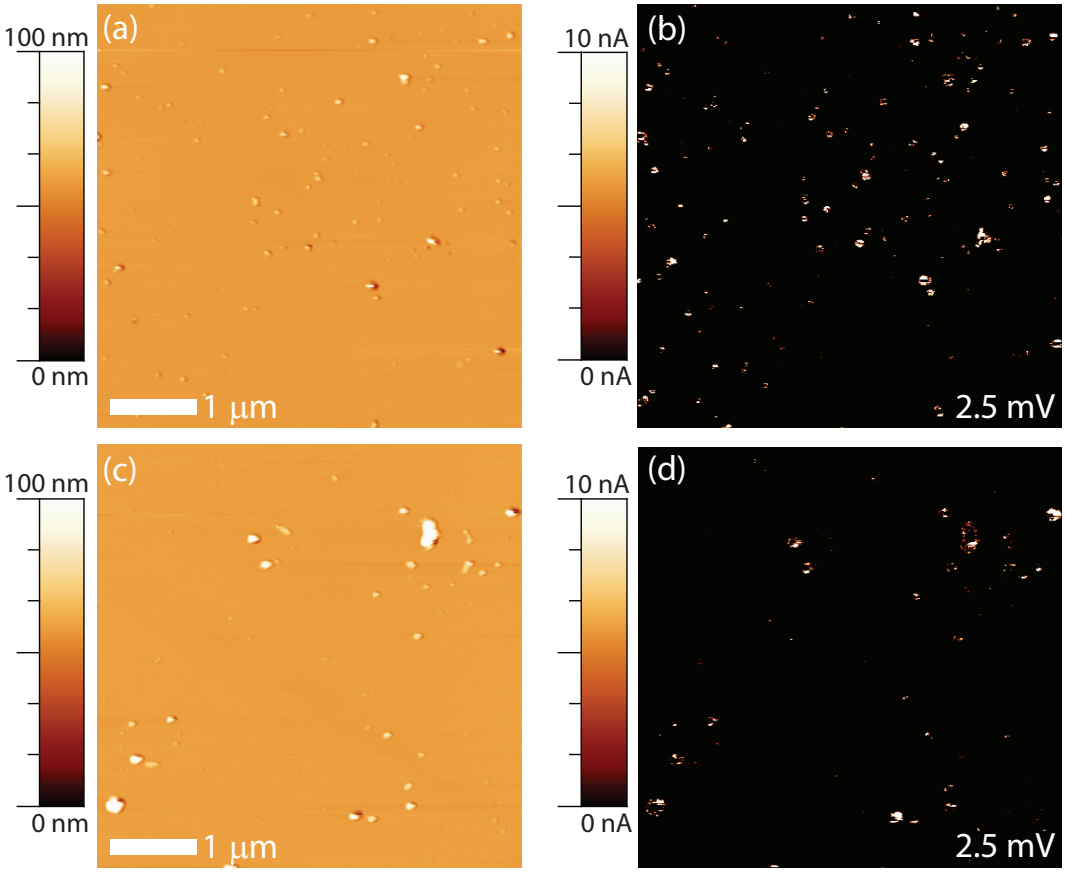

Figure 2. Simultaneously obtained (a) topographical and (b) local current maps of the MgO barrier in non-annealed Fe(20 nm)/MgO on MgO substrate. (c) and (d): the same for a 60 nm-thick lower Fe layer. The density of nanohills are $\sim 6.0\ \mu\text{m}^{-2}$ in Fe(20 nm)/MgO and $\sim 3.6\ \mu\text{m}^{-2}$ in Fe(60 nm)/MgO.

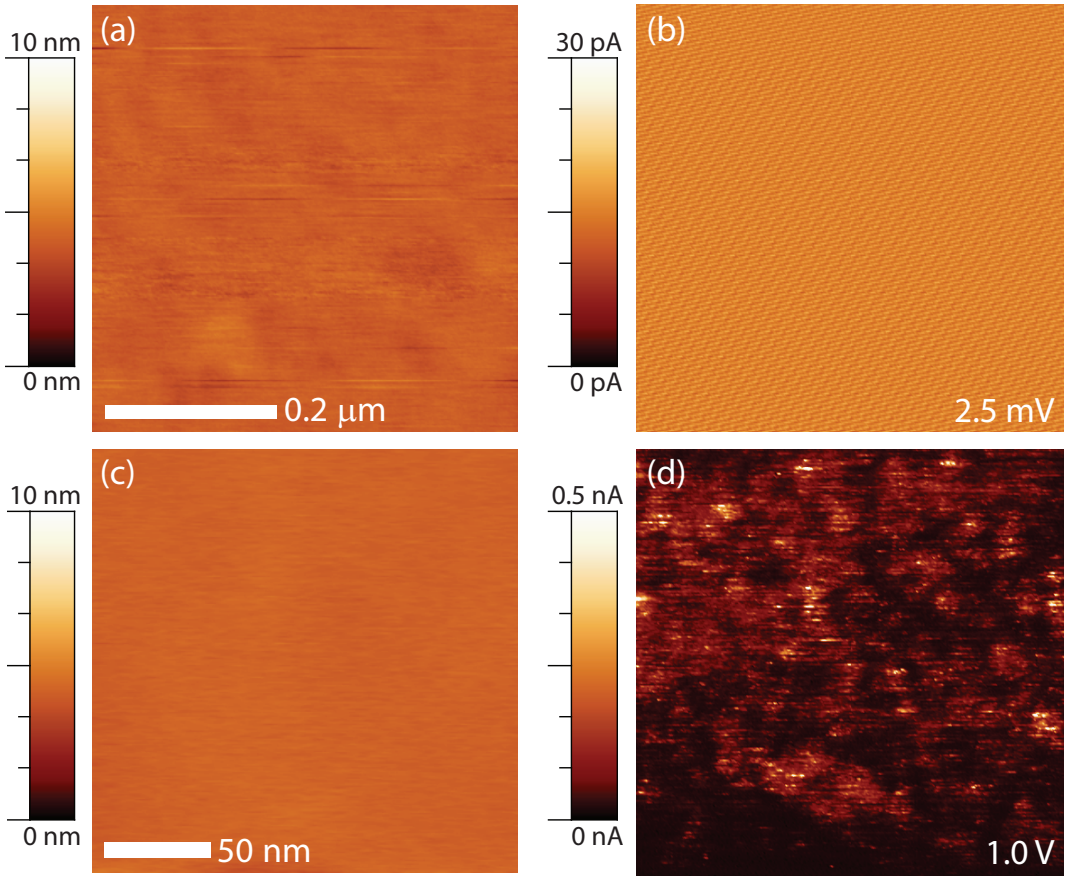

Figure 3. The simultaneous topographical [(a) and (c)] and local current maps [(b) and (d)] of MgO barrier in annealed Fe(20 nm)/MgO samples. (b) and (d) were measured at 2.5 mV and at 1.0 V, respectively.

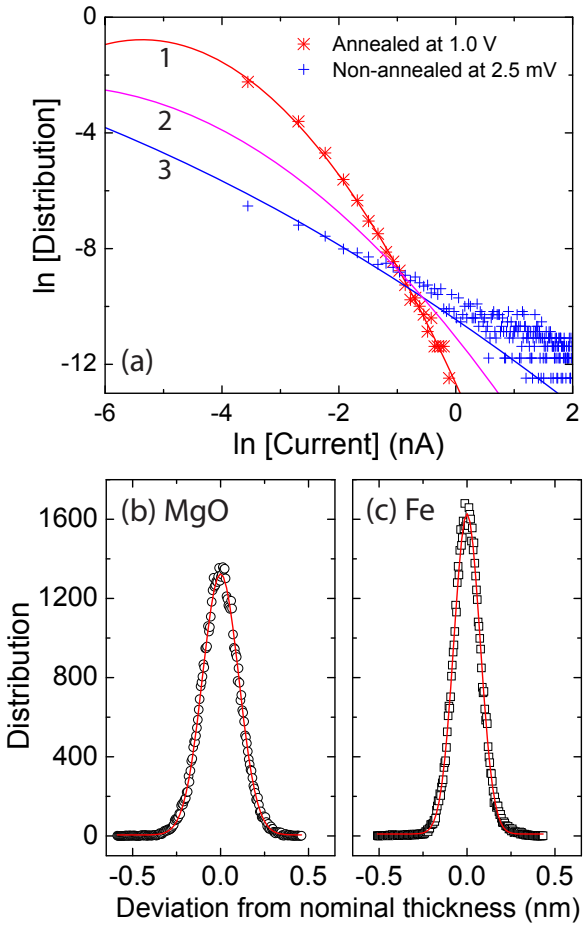

Figure 4. (a) Distributions of local current in an annealed sample at 1.0 V and a non-annealed sample at 2.5 mV. Solid lines show the current distributions with (1) $\mu = -4.16$ and $\sigma^2 = 1.21$, (2) $\mu = -4.16$ and $\sigma^2 = 2.72$, and (3) $\mu = -4.16$ and $\sigma^2 = 10.89$. Distributions of topographical deviation from the nominal thickness of (b) the MgO barrier and (c) the lower Fe layer, and their Gaussian fits.